Anisotropy, multivalency and flexibility-induced effects in colloidal systems

Verweij, R.W.

5 Flexibility-induced effects in the diffusion of colloidal trimers

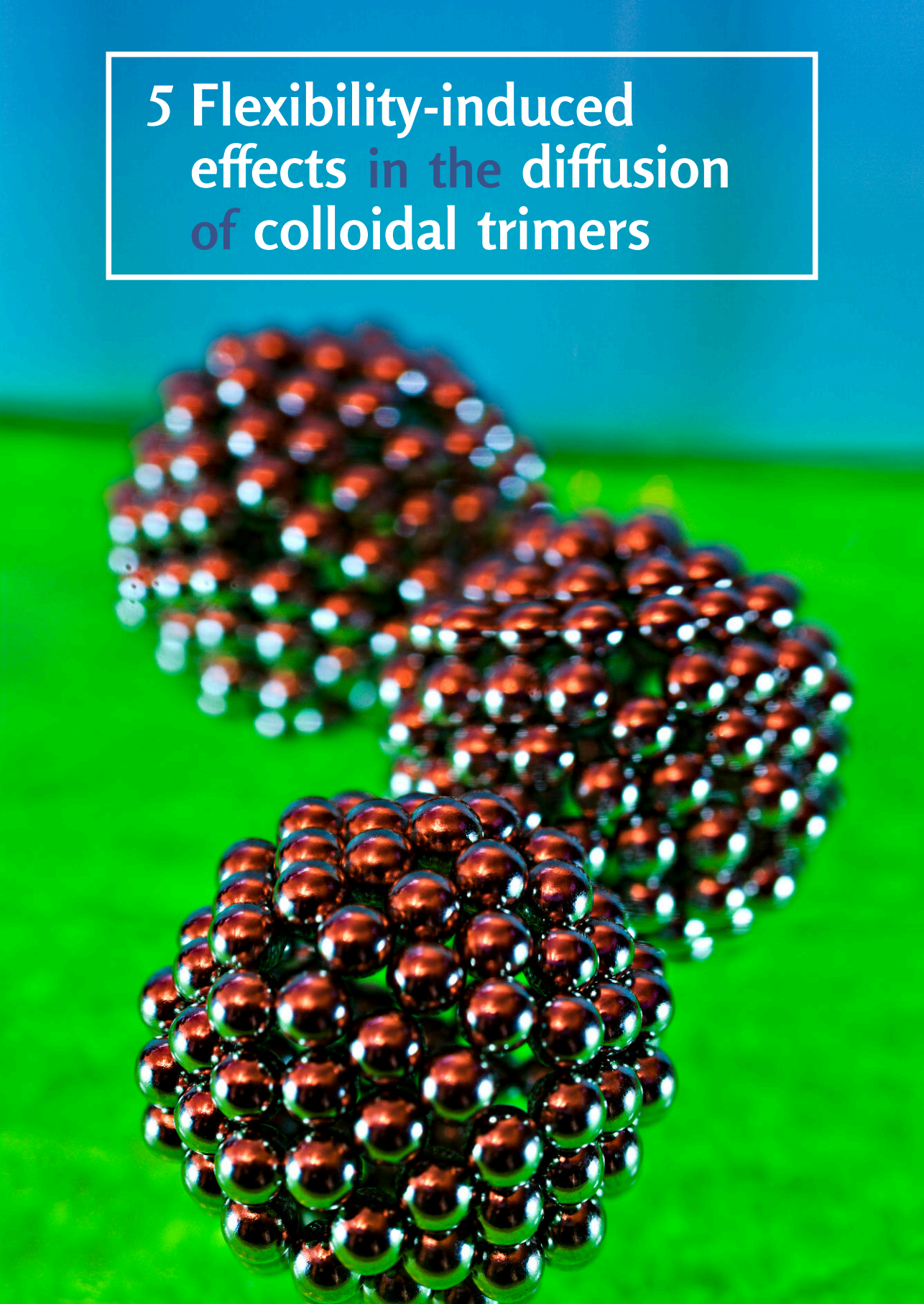

Shape changes resulting from segmental flexibility are ubiquitous in molecular and biological systems, and are expected to affect both the diffusive motion and (biological) function of dispersed objects. The recent development of colloidal structures with freely-jointed bonds have now made a direct experimental investigation of diffusive shape-changing objects possible. Here, we show the effect of segmental flexibility on the simplest possible model system, a freely-jointed cluster of three spherical particles, and validate longstanding theoretical predictions. We find that in addition to the rotational diffusion time, an analogous conformational diffusion time governs the relaxation of the diffusive motion, unique to flexible assemblies, and that their translational diffusivity differs by a small but measurable amount. We also uncovered a Brownian quasiscallop mode, where diffusive motion is coupled to Brownian shape changes. Our findings could have implications for molecular and biological systems where diffusion plays an important role, such as functional site availability in lock-and-key protein interactions.

5.1 Introduction

Many (macro)molecular systems display segmental flexibility, e.g. biopolymers such as transfer RNA,[251] intrinsically disordered proteins,[252] myosin,[251] immunoglobulins,[251] and other antibodies.[101,103,253,254] For most of these systems, the flexibility not only affects the motion of the complex but also its (biological) function.[100–104] For example, proteins often function through shape-dependent lock-and-key interactions where active sites of enzymes are reshaped during the interaction, leading to an induced fit.[255] Additionally, enzymes like adenylate kinase can accelerate biochemical reactions with remarkable specificity and efficacy thanks to a flexible “lid" that opens and closes at each reaction cycle. Because shape has a large effect on the diffusive motion of structures at the short timescales relevant to these reactions, it is expected that the diffusion of reconfigurable objects is different from rigid ones.[251,256–258] Moreover, Adeleke-Larodo et al.[155] recently proposed that changes in an enzymes flexibility upon substrate binding could be responsible for the observed enhanced diffusion of active enzymes.[259,260] Therefore, a rigorous understanding of enzyme function and diffusion requires quantitative knowledge of protein flexibility.[261]

However, direct experimental measurements of flexibility in molecular systems are challenging because they require single-molecule measurement techniques with high spatial and temporal resolution. One way to circumvent this problem is to employ colloidal particles, which have been used as model systems for (macro)molecular

structures,[17–19] because of their unique combination of microscopic size and sensitivity to thermal fluctuations. Studies on the Brownian motion of rigid colloids of various shapes such as ellipsoids,[91,95,96] boomerangs,[14,97,98] and clusters[12,13] have revealed that shape affects the diffusive motion at short timescales. Additionally, displacements are larger in directions that correspond to smaller hydrodynamic drag[12–14,16,91,97] and different diffusive modes can be coupled, e.g. helical particles rotate as they translate and vice versa.[99] At longer timescales, the influence of particle shape decreases because of rotational diffusion.[91]

While rigid assemblies have been extensively studied, little is known about the effect of flexibility. In order to numerically and experimentally investigate the effect of segmental flexibility, we study a simple model system consisting of a freely-jointed chain of three spherical colloidal particles, called flexible trimers or "trumbbells".[107,262] Numerical models were proposed to capture the diffusion of segmentally flexible objects[105–107] and the long time diffusive motion was predicted to be determined by the shape average of the instantaneous diffusivities (so called rigid-body approximation[101,263,264]). For the first time, we are able to test these models using direct experimental measurements of the diffusion of colloidal particles, thanks to the recent development of colloidal structures with freely-jointed bonds,[56,85,110,112,194,242,265] and flexible chains.[266] First, we discuss the short-time diffusion tensor of the flexible trimers, which we compared to numerical calculations and found a good agreement. Furthermore, we uncovered a Brownian quasiscallop mode, where diffusive motion is coupled to Brownian shape changes. Next, we considered the diffusive behavior at longer timescales and found that in addition to the rotational diffusion time, an analogous conformational diffusion time governs the relaxation of the diffusive motion, unique to flexible assemblies.

5.2 Methods

5.2.1 Experimental

Flexible clusters of three colloid-supported lipid bilayers (CSLBs) were prepared as described in previous work.[85,110,112,242] To test the generality of the results presented here, we used two particle sizes, namely 1.93 μm and 2.12 μm silica particles, with different methods of functionalization.

The CSLBs consisting of 2.12 μm silica particles were prepared as described in our recent work.[242] Briefly, the particles were coated with a fluid lipid bilayer by deposition of small unilamellar vesicles consisting of 98.8 mol % of the unsaturated phospholipid DOPC ((Δ9-Cis) 1,2-dioleoyl-sn-glycero-3-phosphocholine), 1 mol % of the lipopolymer DOPE-PEG(2000) (1,2-dioleoyl-sn-glycero-3-phosphoethanolamine-N-[methoxy(polyethylene glycol)-2000]) and 0.2 mol % of the dyed lipids TopFluor-Cholesterol (3-(dipyrromethene boron difluoride)-24-norcholesterol) or DOPE-Rhodamine (1,2-dioleoyl-sn-glycero-3-phosphoethanolamine-N-(lissamine rhodamine B sulfonyl)). The bilayer coating was performed in a buffer at pH 7.4 containing 50 mM sodium chloride (NaCl) and 10 mM 4-(2-Hydroxyethyl)-1-piperazineethanesulfonic

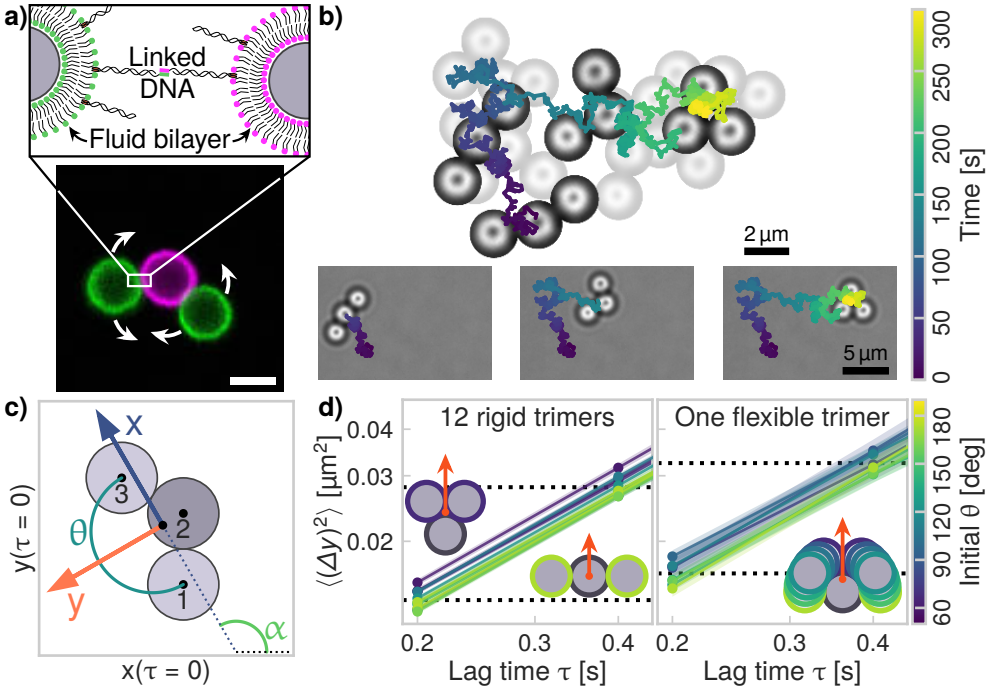

Figure 5.1: **Diffusion of flexible trimers. a)** Schematic (not to scale) of flexible trimers that are self-assembled from colloid-supported lipid bilayers. We inserted DNA linkers into the fluid lipid bilayer surrounding the particle, resulting in bonded particles that can rearrange with respect to each other. Bottom: confocal microscopy image of a flexible trimer. Scalebar is 2 µm. **b)** Overlay of brightfield microscopy images of a flexible trimer with the position of its center of mass as function of time. **c)** Illustration of the body-centered coordinate system. **d)** The mean squared displacement of rigid and flexible trimers. The translational mean squared displacement of flexible trimers in the y-direction is angle dependent for short lag times, at longer lag times this angle dependence is no longer present due to rotational and conformational relaxation, which happens on a shorter timescale than for rigid trimers (raw data).

acid (HEPES). We added double-stranded DNA (of respectively strands DS-H-A and DS-H-B of Table A.1) with an 11 base pair long sticky end and a double stearyl anchor, which inserts itself into the bilayer via hydrophobic interactions (see Figure 5.1a). When two particles with complementary DNA linkers come into contact, the sticky ends hybridize and a bond is formed. Self-assembly experiments were performed in a different buffer of pH 7.4, containing 200 mM NaCl and 10 mM HEPES. We imaged 21 trimers of 2.12 μm CSLBs, that were formed by self-assembly in a sample holder made of polyacrylamide (PAA) coated cover glass. The PAA functionalization was carried out using a protocol[202] which we modified by adding 0.008 mol % bis-acrylamide and performing the coating under a nitrogen atmosphere, both of which resulted in a more stable coating. Using an optical microscope, we imaged the clusters for 5 min at frame rates between 5 fps to 10 fps. Particle positions were tracked using a custom algorithm[242] available in TrackPy by using the `locate_brightfield_ring` function,[188] as depicted schematically in Figure 3.1.

Additionally, we analyzed 9 trimers of 1.93 μm CSLBs, with silica particles purchased from Microparticles GmbH (product code SiO_2−R-B1072). For these particles, we used a similar protocol to form supported lipid bilayers with only 2 minor modifications: first, the lipid composition we used was 98.9 mol % DOPC, 1 mol % DOPE-PEG(2000) and 0.1 mol % DOPE-Rhodamine. Second, we added Cy3-labeled DNA with a self-complementary 12 base pair sticky end and a cholesterol anchor that inserts itself into the lipid bilayer due to hydrophobic interactions. We used the DNA sequence from Leunissen et al.[72] (see Table A.1, strands PA-A and PA-B).

To image the 1.93 μm CSLBs we used a flow cell produced as detailed in the Supplementary of Montanarella et al.[267] As the base of our flow cell we used a single capillary with dimensions 3 cm × 2 mm × 200 μm. To prevent the lipid coated clusters from sticking to the class capillary, we coated the inside of the capillary with poly(2-hydroxyethyl acrylate) (pHEA) polymers. To this end, we first flushed the cell with consecutively 2 mL 2 mM NaOH solution, 2 mL water and 2 mL EtOH. We then functionalized the glass surface with the silane coupling agent 3-(methoxysilyl)propyl methacrylate (TPM) by filling the flow cell with a mixture of 1 mL EtOH, 25 μL TPM, and 5 μL 25 % v/v NH_3 in water and leaving it for 1 hour. We then washed and dried the flow cell by flushing with 2 mL ethanol and subsequently with nitrogen. We grew pHEA brushes from the surface through a radical polymerization by filling the cell with a mixture of 2.5 mL EtOH, 500 μL HEA and 20 μL Darocur 1173 photoinitiator. We initiated the reaction by placing the cell under a UV lamp with wavelength λ = 360 nm for 10 minutes. Finally, we flushed the cells with 10 mL EtOH or Millipore filtered water. We stored the coated cells filled with EtOH or Millipore filtered water and for no more than one day. Self-assembly experiments were performed in a buffer of pH 7.4, containing 50 mM NaCl and 10 mM HEPES. We imaged 9 freely-jointed trimers and 13 rigid trimers stuck in various opening angles shown in Figure 5.2 for 30 minutes with a frame rate of 5 fps. Particle positions were tracked using the 2007 Matlab implementation by Blair and Dufresne of the Crocker and Grier tracking code.[189]

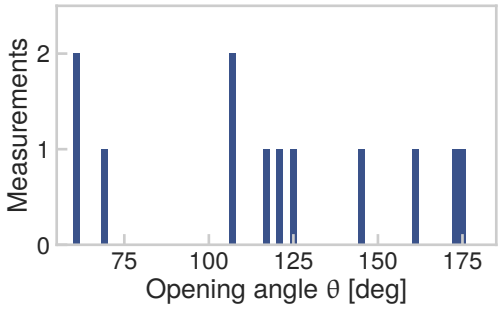

Figure 5.2: **Opening angles of rigid trimers.** The number of rigid clusters of different opening angles used in this study. Six rigid trimers have a 'compact' opening angle (below 120°) while the other six are more extended.

5.2.2 Diffusion analysis

For all analysis, we only selected trimers that showed all bond angles during the measurement time, experienced no drift and were not stuck to the substrate. After the particle positions were tracked, we determined the short-time diffusivity of the trimers as described by Equation 5.4 separately for all trimers. For each pair of frames, we determined the initial average opening angle $\overline{\theta}$ of the trimer between t and $t+\tau_{\text{short}}$, with $\tau_{\text{short}} = 0.25\,\text{s}$. Then, we stored the diffusion tensor elements separately for each initial opening angle. For short times up to $\tau_{\text{short}} = 0.25\,\text{s}$, we used a bin size of 15° while for longer times, we used two bins of 60° covering the range of $[60°, 120°)$ and $[120°, 180°]$. We scaled each element with the friction factors we obtained for that measurement, based on the diffusion coefficient for lag times up to τ_{short}. The average diffusion tensor elements were then obtained by fitting the overall slope of the mean (squared) displacements of all the individual diffusion tensor elements as a function of lag time (see Figure 5.9a, c, e and Figure 5.11a, c). We used a linear function (with zero intercept) divided into ten segments with slopes $2D_i$ (spaced evenly on a log scale), which correspond to the ith diffusion coefficient for those lag times. This resulted in the average diffusion tensor for all binned average opening angles $\overline{\theta}$ as a function of the lag time τ. For fitting, we used a standard least squares method and we estimated the error using a Bayesian method to find an estimate of the posterior probability distribution, by using a Markov chain Monte Carlo (MCMC) approach as implemented in the Python packages lmfit[246] and emcee.[207] We estimated the autocorrelation time τ_{acor} of the chain using the builtin methods and ran the analysis for at least $100\tau_{\text{acor}}$ steps, where we discarded the first $2\tau_{\text{acor}}$ steps (corresponding to a burnin phase) and subsequently used every other $\tau_{\text{acor}}/2$ steps (known as thinning). The reported values correspond to the maximum likelihood estimate of the resulting MCMC chain, the reported uncertainties correspond to the minimum and maximum of the obtained posterior probability distribution.

5.2.3 Hydrodynamic modeling

The diffusion of segmentally flexible objects can be described using hydrodynamic modeling.[107,268] To compare our experimental results to these predictions, we followed the procedure described by Harvey and coworkers.[107] Of the seven degrees

of freedom in three dimensions (three translational, three rotational, one internal degree of freedom), we considered only the four degrees of freedom of interest for our quasi-two dimensional system of sedimented clusters. Briefly, following the method outlined by Harvey and coworkers,[107] we determined the hydrodynamic resistance (or friction) tensor $\boldsymbol{R}_0$ with respect to the central particle. Using this resistance tensor, we calculated the diffusion tensor $\boldsymbol{D}_0 = kT\boldsymbol{R}_0^{-1}$, to which we apply the appropriate coordinate transformation to obtain the 7×7 diffusion tensor $\boldsymbol{D}_{\text{c.m.}}$ relative to the center of mass of the cluster. We chose the center of mass as reference point because it is a good approximation of the center of diffusion of a flexible particle: in fact, it was found to be a better choice than either the center of diffusion or resistance of a rigid cluster of the same shape.[107] In Chapter 6, we will discuss how to calculate the center of diffusion for a flexible cluster[269] and what effect it has on the diffusion tensor when used as a tracking point instead of the center of mass. Additionally, we have calculated the diffusion tensor with respect to the central particle and these results are shown in Figure 5.7.

The diffusivity of flexible colloidal clusters can be modeled using bead or bead-shell models.[270] We used three different models to describe the hydrodynamic properties of the flexible trimers: a bead model (Figure 5.3a), a bead-shell model for a rigid trimer using HydroSub[263] (Figure 5.3b) and a bead-shell model for flexible trimers (Figure 5.3c). For the bead model, we modeled the trimer using three beads (diameter of 2 μm). For the bead-shell models, we modeled the trimer using approximately 2500 to 9500 smaller beads with bead radii ranging from 54 nm to 31 nm respectively, where the beads where placed to form three 2 μm shells. We followed existing methods[271,272] for constructing the bead shell model: to summarize, the positions of the small beads were calculated by placing them on concentric circles, starting at the equator of an individual 2 μm sphere and continuing the process towards the poles of the sphere using circles of decreasing radius and finally putting one sphere at each of the poles. Three spherical bead-shell models were then put together to form a trimer and we removed overlapping beads at the contact points between the particles. The results were evaluated for multiple small bead sizes, so that the result could be linearly extrapolated[271,272] to the limit where the small bead radius approaches zero.

In Figure 5.3d, the calculated diffusivities are shown for all three models. The bead model predicts higher diffusivities compared to both bead-shell models for all different elements of the diffusion tensor. The bead-shell models agree qualitatively, but predict different magnitudes of the diffusivities due to differences in hydrodynamic interactions between the outer beads, which are higher for the flexibly-linked clusters.[251,256–258]

Because drag forces act on the surface of the particles, the bead-shell model is more accurate in describing the diffusive properties of the clusters.[263,271,272] The accurate consideration of hydrodynamic effects was found to be important for the segmentally flexible system we study: hydrodynamic interactions lead to a slower decay of the autocorrelation of the particle shape[273] and lead to an increase in the translational diffusivity.[101,251] We have used the bead-shell model of Figure 5.3c (solid

line) to model our experimental data, because it best describes our experimental data and because it can be used to model conformational changes, which are not yet implemented in the HydroSub model.

To calculate the diffusion tensor elements, we used the Rotne-Prager-Yamakawa (RPY) interaction tensor[34,275] $\boldsymbol{T}_{ij}$ to model hydrodynamic interactions between particles i and j:

$$\boldsymbol{T}_{ij} = \frac{1}{8\pi\eta_0 R_{ij}} \left[\boldsymbol{I} + \frac{\boldsymbol{R}_{ij}\boldsymbol{R}_{ij}}{R_{ij}^2} + \frac{2\sigma^2}{R_{ij}^2} \left(\frac{\boldsymbol{I}}{3} - \frac{\boldsymbol{R}_{ij}\boldsymbol{R}_{ij}}{R_{ij}^2} \right) \right], \tag{5.1}$$

where σ is the particle radius, $\boldsymbol{R}_{ij}$ is the vector between particles i and j, $\boldsymbol{I}$ is the 3×3 identity matrix, η_0 is the viscosity of the medium. Using the RPY tensor prevents singularities that may lead to the large, nonphysical numerical fluctuations[276] found when using lower order terms (Oseen tensor), higher order terms or multi-body effects.[277]

We used the RPY tensor to model the hydrodynamic interactions between the beads and followed the procedure outlined by Harvey and coworkers[107] to obtain the diffusion tensor, as explained in Section 5.3. This was done for all small bead radii and we used a linear extrapolation to zero bead size to obtain the final diffusion tensor elements.[271,272] Additionally, we used HydroSub[263] to model the diffusivity of rigid trimers of the same opening angles.

Near-wall diffusion: friction factors

Here, we have modeled the effect of the substrate using simple friction scaling factors. A comparison with more sophisticated simulations that take hydrodynamic interactions between the particles and the wall into account is given in Chapter 6. The three friction correction factors that account for substrate friction were determined in the following way:

$$\begin{aligned} \phi_{tt} &= \left\langle \boldsymbol{D}[tt]_t / (\sigma_e \boldsymbol{D}[tt]_{e,0}) \right\rangle \\ \phi_{(\alpha\alpha,\theta\theta)} &= \left\langle \boldsymbol{D}[(\alpha\alpha,\theta\theta)]_t / (\sigma_e^3 \boldsymbol{D}[(\alpha\alpha,\theta\theta)]_{e,0}) \right\rangle \\ \phi_{ij} &= \sqrt{\phi_{ii}\phi_{jj}} \quad \text{for} \quad i \neq j, \end{aligned} \tag{5.2}$$

where $\boldsymbol{D}[ij]_k$ denotes the theoretical ($k = t$) or experimental ($k = e$) diffusion tensor element and σ_e the experimental particle radius. The subscript tt denotes the translational component of the diffusivity. These factors were determined separately for each experiment, because differences in surface and particle functionalizations resulted in differences in substrate-particle and particle-particle friction, that in turn affect the diffusivity of the cluster. We separated the correction factors into these three factors because different modes of diffusion are expected to lead to different amounts of friction with the substrate.[154]

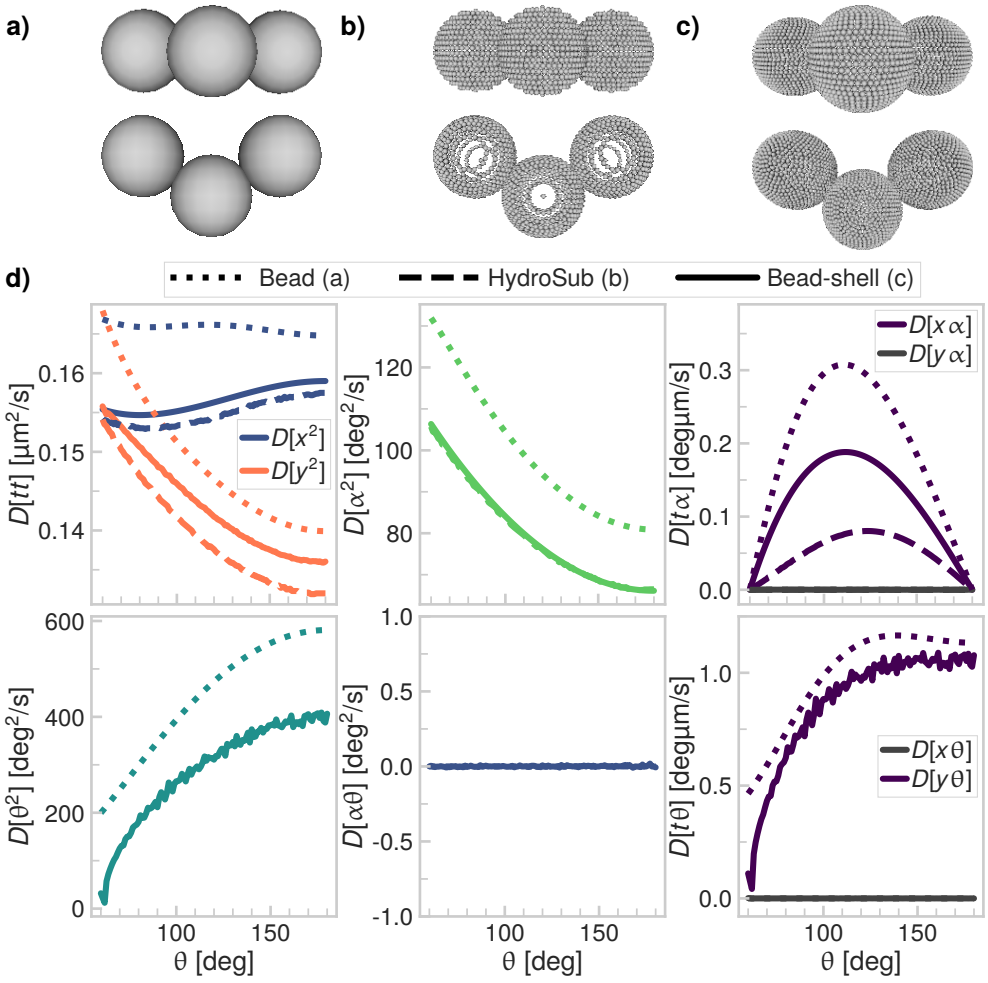

Figure 5.3: **Comparison of the diffusion tensor calculated by different hydrodynamic models.** Renderings made using FreeWRL[274] of **a)** the simple bead model, **b)** the bead-shell model (minimum radius of the small spheres $r = 55\,\text{nm}$) used by HydroSub[263] for rigid trimers, **c)** the bead-shell model (radius of the small spheres $r = 31\,\text{nm}$ to $54\,\text{nm}$, $r = 45\,\text{nm}$ is shown) we used for calculating hydrodynamic properties of flexible trimers. For all models, the radius of the large particles is $R = 1\,\mu\text{m}$. **d)** Top row, left to right: the translational diffusivity, rotational diffusivity and coupling between translational and rotational diffusivity for the bead model (a, dotted lines), the rigid bead-shell model generated with HydroSub (b, dashed lines) and the segmentally flexible bead-shell model (c, solid lines). Bottom row, left to right: the joint flexibility, coupling between shape changes and rotation and couplings between shape changes and translational diffusion.

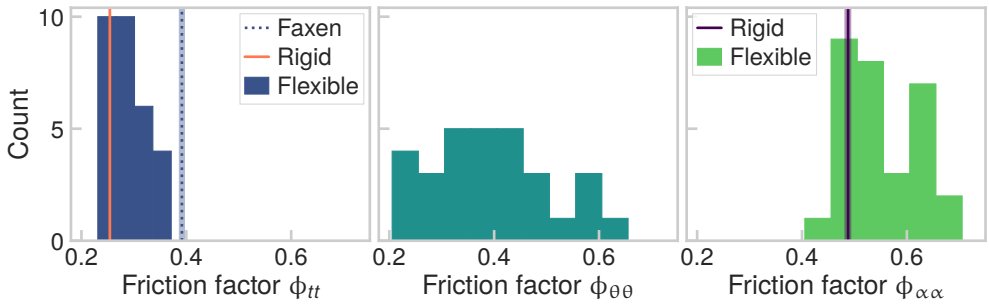

Figure 5.4: **Distribution of friction factors** as given by Equation 5.2. The mean value for $\phi_{tt} = 0.29 \pm 0.04$ is close to the lower bound of 0.39 (indicated by the dotted line, left plot) as predicted by Equation 5.3. We find an average rotational friction factor $\phi_{\alpha\alpha} = 0.55 \pm 0.07$ (center plot). The average flexibility friction factor $\phi_{\theta\theta} = 0.40 \pm 0.12$ shows a broader distribution, which we attribute to a spread in DNA linker concentration (right plot). The average friction factor of the rigid clusters is also indicated (left and right plots, $\phi_{tt,r} = 0.254 \pm 0.004$, $\phi_{\alpha\alpha,r} = 0.49 \pm 0.02$) and coincides with the friction factors we find for flexible clusters.

As a first approximation to compare the experimental diffusion of freely-jointed trimers above a substrate to models of trimers diffusing in the bulk, we use Faxen's theorem:[192]

$$\frac{D_w(h)}{D_0} = 1 - \frac{9}{16}\frac{R}{h+R} + \frac{1}{8}\left(\frac{R}{h+R}\right)^3 - \frac{45}{256}\left(\frac{R}{h+R}\right)^4 + O\left(\left(\frac{R}{h+R}\right)^5\right), \tag{5.3}$$

with D_0 the translational diffusion coefficient in the bulk, $D_w(h)$ the in-plane translational diffusion coefficient near a wall at height h and R the particle radius. We calculate an effective particle radius

$$R_{\text{eff}} = \frac{k_B T}{6\pi\eta D} = 1.8\,\mu\text{m}$$

from the short-time translational diffusion coefficient,[278] with k_B Boltzmann's constant, T the temperature, η the viscosity of the medium and $D = 0.136\,\mu\text{m}^2\,\text{s}^{-1}$ the lowest short-time translational diffusion coefficient of the trimer as predicted by the bead-shell model.

The expected Debye length[20] of our medium (at $I = 200\,\text{mM}$) is

$$\kappa^{-1} = \frac{0.304}{\sqrt{I}} \approx 0.7\,\text{nm}$$

and so we neglect electrostatic interactions between the trimer and substrate. Therefore, the height of the particle above the substrate is set by balancing the effect of

sedimentation and thermal fluctuations as expressed by the gravitational length l_g:

$$l_g = \frac{k_B T}{g \Delta \rho V},$$

with g the gravitational acceleration constant, $\Delta\rho$ the density difference between the particle and the medium and V the volume of the particle.

Using the appropriate values for the trimer, we find $l_g = 20\,\text{nm}$. By setting this as input for h in Equation 5.3, we obtain a upper bound for $D_w(h)/D_0$, equal to 0.40. A lower bound is found at $h = 0$, which gives a value of 0.39. The translational friction coefficient $D_w(h)/D_0$ that we find has an average value of 0.29 ± 0.04, as shown in Figure 5.4, which is close to the lower bound we have calculated above. The experimental value is slightly lower than the predicted lower bound, because Equation 5.3 accounts for hydrodynamic interactions only and real experiments typically show lower diffusivities because of additional sources of friction,[279] which in the present case could be explained by additional friction between the polymer coating and the particles. Moreover, a comparison with more sophisticated simulations that take hydrodynamic interactions between the particles and the wall into account is given in Chapter 6.

5.3 Results and Discussion

5.3.1 Short-time Brownian motion of flexible trimers

The flexibly-linked colloidal trimers are made by self-assembly of colloid-supported lipid bilayers (CSLBs).[85,110,112,242] Briefly, spherical colloidal silica particles are coated with a fluid lipid bilayer. DNA linkers with complementary sticky ends are inserted into the bilayer using a hydrophobic anchor. The particles are self-assembled by hybridization of the DNA sticky ends, which provide strong and specific interactions. The trimers are freely-jointed because the DNA linkers can diffuse on the fluid lipid bilayer that surrounds the particles (see Figure 5.1a). The clusters undergo translational and rotational diffusion while they are also free to change their shape (see Figure 5.1b and Supplementary Movie 1 of Verweij & Moerman *et al.*[244]). For simplicity, we used heavy silica particles so that their mobility is confined to the bottom of the container by gravity, which leads to two-dimensional Brownian motion.

For rigid objects in two dimensions, the diffusive motion can be described by a 3×3 diffusion tensor calculated from the linear increase of the mean squared displacements of the particle as function of lag time.[31] For flexible objects, this diffusion tensor has to be extended with an additional degree of freedom[107] for each internal deformation mode (here: one), and we therefore consider the 4×4 diffusion tensor $\boldsymbol{D}[ij]$. Here, $i, j \in [x, y, \alpha, \theta]$ are elements of a body-centered coordinate system (see Figure 5.1c) at the center of mass. We chose the center of mass as reference point, because for flexible objects, it is more appropriate than either the center of diffusion or resistance of a rigid cluster of the same shape.[107] In Chapter 6, we will discuss how to calculate the center of diffusion for a flexible cluster[269] and what effect it has on

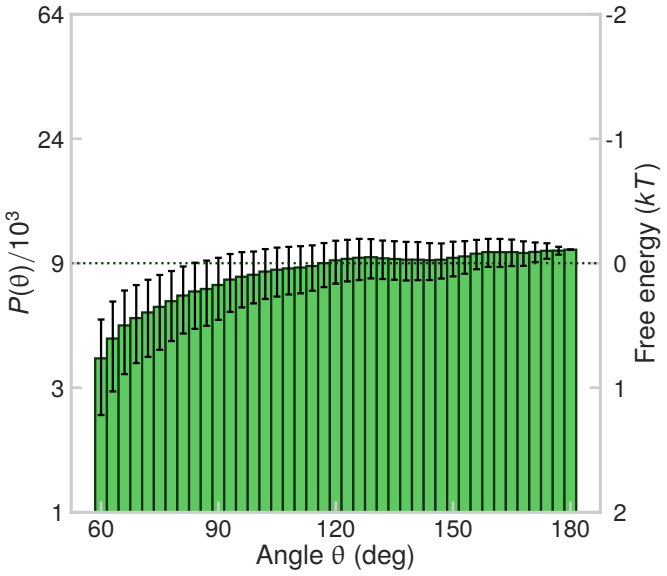

Figure 5.5: **Probability and free energy as a function of the opening angle of flexible trimers.** Probability and corresponding free energy of the opening angle of the flexible trimers used in this work (with the reference set at 180°). There is no preference for a specific opening angle within the experimental error, meaning the particles are freely-jointed, as was shown before.[242] Note that the slightly lower probability at angles smaller than $60° + \sqrt{2J\tau} \approx 69°$ (with J the joint flexibility and τ the sampling interval) is caused by boundary effects inherent to our analysis method.[242]

the diffusion tensor when used as a tracking point instead of the center of mass. In the coordinate system used here, the y-axis is perpendicular to the end-to-end vector and points away from the central particle, and the direction of the x-axis is chosen to form a right-handed coordinate system. We label the opening angle of the trimer θ and the (anticlockwise) rotation angle of the x-axis with respect to the lab frame α. We align the lab frame such that it coincides with the body-centered coordinate system at $\tau = 0$.

Shape determines the diffusion tensor for rigid objects and therefore we expect it to be important for flexible objects as well, but due to its flexibility, the cluster shape is continuously changing. Therefore, we categorize the trajectories by their (initial) average opening angle $\overline{\theta}$ of the smallest lag time interval and we use angular bins to summarize the results. The short-time diffusion tensor is calculated from experimental measurements in the following way:

$$\boldsymbol{D}[ij](\overline{\theta}) \equiv \frac{1}{2}\phi_{ij}\frac{\partial\langle\Delta i\Delta j\rangle_\tau}{\partial\tau}, \tag{5.4}$$

with τ the lag time between frames, $\langle\cdots\rangle_\tau$ denotes a time average over all pairs

of frames τ apart and $\Delta i = i(t + \tau) - i(t)$, ϕ_{ij} is a correction factor that accounts for particle-particle and particle-substrate friction (see Section 5.2.3 and Figure 5.4). The correction factors ϕ_{ij} are a first-order approximation to model the wall effect of the glass surface, that for translational diffusion agrees closely with predictions from hydrodynamic theory, as shown in Figure 5.4. A comparison with more sophisticated simulations that take hydrodynamic interactions between the particles and the wall into account is given in Chapter 6. We evaluated Equation 5.4 at $\tau = 0.25s$, set by the frame rate of our camera.

Using Equation 5.4, the resulting shape and time dependent translational diffusivity in the y-direction of twelve rigid and one flexible trimer are shown in Figure 5.1d. Initially, at short timescales, there is a clear effect of cluster shape for both flexible and rigid trimers: translational diffusion in y is highest for compact shapes. In comparison to rigid trimers, the diffusivity of the flexible trimer is slightly enhanced. Two other features unique to flexible clusters are that using a measurement of only one cluster, all possible cluster shapes are sampled and that the effect of shape vanishes on a much shorter timescale compared to the rigid clusters.

To study the diffusivity more carefully, we determined the average short time diffusion tensor of thirty flexible trimers. As shown in Figure 5.6a, the diffusion tensor elements were obtained by fitting the slope of the mean squared displacement versus lag time. We find three features that are in line with previous findings for rigid clusters[13] and that give confidence in the used analysis: first, translational diffusivity is higher along the longitudinal x-direction compared to the lateral y-direction (Figure 5.6d). Additionally, the rotational diffusivity shown in Figure 5.6b is higher for compact trimers as opposed to fully extended trimers and we observe a coupling between translational diffusion and rotational diffusion in the x-direction (Figure 5.6e).

However, flexibility gives rise to other modes that are not present in rigid assemblies. We found that the flexibility itself, as shown in Figure 5.6c, increases as function of the opening angle, leading to a four fold increase of flexibility for extended shapes compared to closed shapes. It is most likely caused by hydrodynamic interactions between the outer particles, as was predicted by earlier works.[106]

Even more strikingly, the hydrodynamic drag on the outer particles leads to an increase in opening angle θ for positive displacements along the y-axis (Figure 5.6f), which we call the Brownian quasiscallop mode. This Brownian quasiscallop mode may have implications for the accessibility of the functional site in induced fit lock-and-key interactions commonly observed in proteins.[255] We stress that this correlation does not lead to self-propulsion because it has time reversal symmetry. As the opening angle θ increases, the location of the center of mass moves in the negative y-direction of the original particle coordinate system. Therefore, this correlation is larger when the central particle is chosen as the origin of the coordinate center.

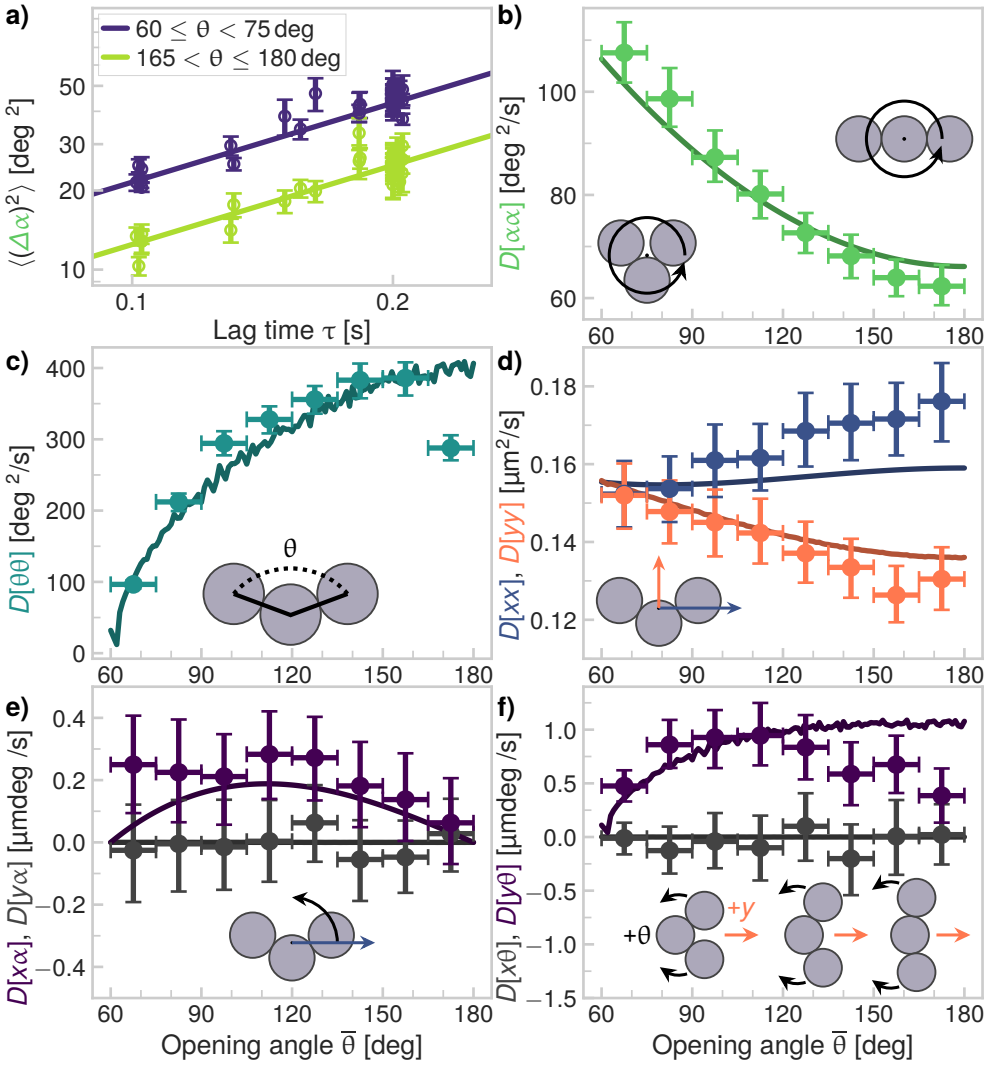

Figure 5.6: **Short-time translational, rotational, internal and coupled diffusivity** of flexible trimers (up to 0.25 s). **a)** Mean squared rotational displacements for lag times up to $\tau = 0.25$ s, for two different instantaneous opening angles $\overline{\theta}$. **b)** The rotational diffusivity is highest for the most compact shapes. **c)** The joint flexibility increases as function of opening angle θ. **d)** While equal for bent trimers, the translational diffusivity along the long axis (x) is higher than along the short axis (y). **e)** We find a correlation between counterclockwise rotation and positive x displacements. **f)** There is a coupling between translational diffusion in the y-direction and shape changes: as the cluster diffuses in the positive y-direction, the angle θ increases, leading to a Brownian scallop-like motion at short timescales. In panels b-f, the scatter points show the experimental measurements and the lines show the numerical calculations based on Harvey et al. [107]

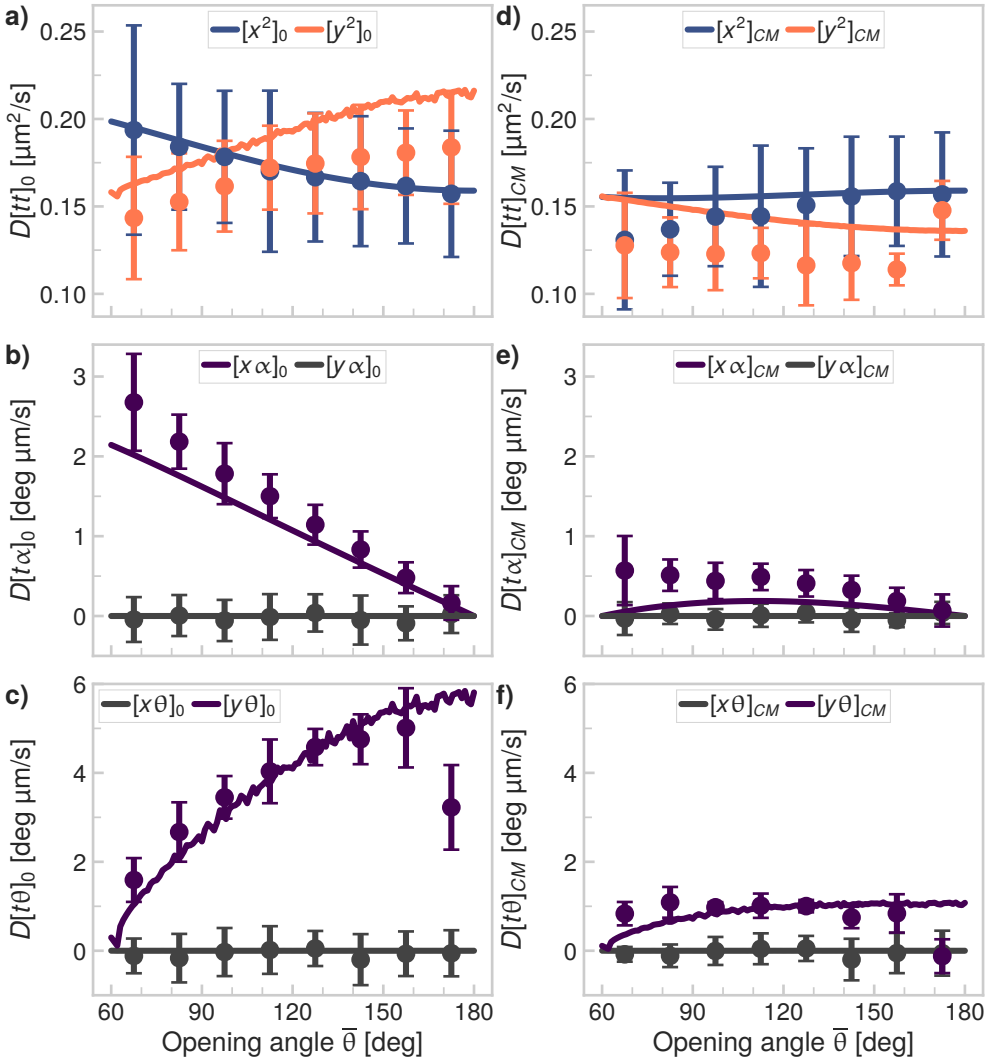

Figure 5.7: **Influence of the reference point on the diffusion tensor. a-c)** The translational (a), translational-rotational (b) and translational-conformational (c) diffusivities with the reference point chosen in the center of the central particle. **d-f)** The translational (d), translational-rotational (e) and translational-conformational (f) diffusivities with the reference point at the center of mass of the cluster. For these graphs, we transformed the data from panels a-c using the coordinate transformation described in the text from the "center particle"-based to the "center of mass"-based diffusivity. Note that the combination of experimental errors of the $D[t\alpha]$, $D[\alpha^2]$, $D[t\theta]$, $D[\theta^2]$ and $D[\alpha\theta]$ terms lead to large uncertainties and deviations, especially for the translational diffusivities. In all panels, the points show the experimental data and the lines are the predictions of the bead-shell model.

The influence of the tracking point

For purely rotational and conformational terms, the diffusivity is expected to be independent of the chosen reference point, however, for terms that include translation, the location of the reference point has a large effect on the measured diffusivity.[105,107] This can be seen in Figure 5.7: in panels a-c), we show the diffusivities calculated using the central particle as reference point. The results are remarkably different from the center of mass based results shown in Figure 5.7d-f), where we have used the diffusivities relative to the central particle to calculate the diffusivities relative to the center of mass using the coordinate transformations determined by Harvey and coworkers[107]:

$$\begin{aligned} D[tt]_{CM} = D[tt]_0 &+ D[t\alpha]_0^{\intercal} \cdot U - U \cdot D[t\alpha]_0 + U \cdot D[\alpha^2] \cdot U \\ &+ D[t\theta]_0^{\intercal} \cdot W + W^{\intercal} \cdot D[t\theta]_0 - U \cdot D[\alpha\theta]^{\intercal} \cdot W \\ &+ W^{\intercal} \cdot D[\alpha\theta] \cdot U + W^{\intercal} \cdot D[\theta^2] \cdot W \end{aligned} \tag{5.5}$$

$$D[t\alpha]_{CM} = D[t\alpha]_0 + D[\alpha^2] \cdot U + D[\alpha\theta]^{\intercal} \cdot W \tag{5.6}$$

$$D[t\theta]_{CM} = D[t\theta]_0 + D[\alpha\theta] \cdot U + D[\theta^2] \cdot W \tag{5.7}$$

We have made this comparison because the coupling terms are expected to be larger in the central particle frame. The results indeed show this larger coupling and exclude the possibility that the coupling modes we observed are artifacts of the coordinate system we used. In Chapter 6, we will discuss how to calculate the center of diffusion for a flexible cluster[269] and what effect it has on the diffusion tensor when used as a tracking point instead of the center of mass.

Because the rotational and conformational diffusivities are independent of the reference point, localization uncertainties in the determination of the position of the reference point may have a larger effect on $D[xx, yy, xy, x\alpha, y\alpha, x\theta, y\theta]$ than on $D[\alpha^2, \theta^2, \alpha\theta]$. Because of the uncertainties that are propagated when we first determine the diffusivity with respect to the central particle and then transform this to the diffusivity with respect to the center of mass (in Figure 5.7d-f), the error is larger for this method compared to the direct calculation of the diffusivities with respect to the center of mass. Therefore, the latter method should be preferred.

In summary, our experimental data allow us to test for the first time theoretical predictions made by Harvey and coworkers,[107] who modeled the diffusion of segmentally flexible objects by calculating the hydrodynamic interactions between two sub units. We applied their calculations to a bead-shell model, adapted to match the conditions of our experiments (see Section 5.2.3 and Figure 5.3) and find good agreement between the numerical calculations and the experimental data. The good agreement between the numerical results and the experimental data validates their model for the diffusivity of microscopic objects with internal degrees of freedom. For some angles and entries of the diffusion tensor, the experimental data shows small deviations from the predicted model values, especially for translational diffusion, the Brownian quasiscallop mode and the flexibility (see Figure 5.6c, d and f). We

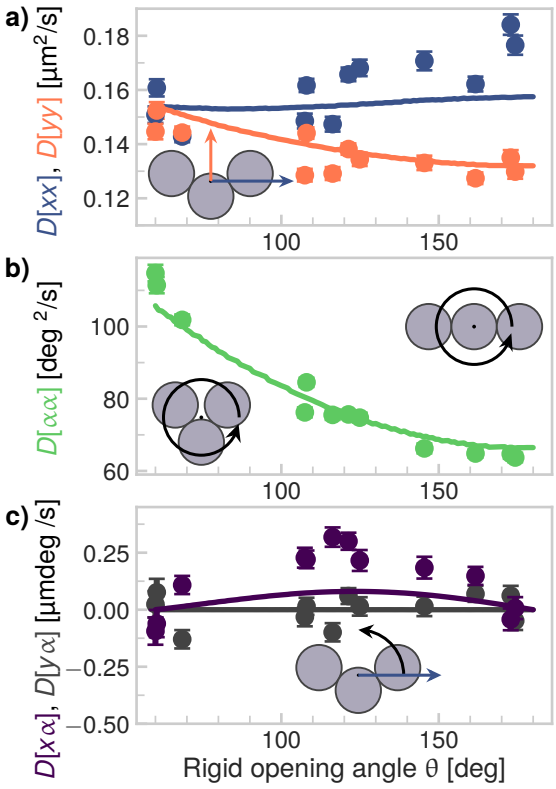

Figure 5.8: **Short-time diffusion of rigid trimers.** The **a)** translational, **b)** rotational and **c)** translational-rotational diffusivities of rigid trimers with various opening angles (see Figure 5.2 for details). In all panels, the points correspond to the experimental diffusivities (up to lag times of $\tau = 0.25\,\mathrm{s}$) and the solid lines correspond to the numerical calculations performed using HydroSub,[263] as detailed in Figure 5.3. All points are scaled by the same average friction factor as shown in Figure 5.4 in order to compare the experiments to the numerical simulations.

hypothesize that these differences may arise because the numerical calculations do not take particle-particle and particle-substrate friction into account, other than as a first-order approximate scaling using the friction factors ϕ_{ij} as defined in Equation 5.4. For example, substrate interactions were found to lead to enhanced diffusion for a model dumbbell consisting of two hydrodynamically coupled subunits.[104] More elaborate models may be used to provide higher-order corrections to the model we used here,[35] however their validity for flexible objects needs to be investigated. Moreover, our model also does not account for some out-of-plane diffusive motions against gravity, that might occur in the experiments. We will discuss these effects in greater detail in Chapter 6.

5.3.2 Flexible trimers compared to rigid trimers

In addition to flexibly-linked trimers of CSLBs, we have also studied rigid trimers of CSLBs that are frozen in a specific shape, as shown in Figure 5.2. First, we have compared their short-time diffusivity as function of their shape to bead-shell model calculations performed using HydroSub.[263] As shown in Figure 5.8, bead-shell models accurately describe their translational (Figure 5.8a), rotational (Figure 5.8b) and translational-rotational (Figure 5.8c) short-time shape-dependent diffusivities.

Then, we compared the short-term translational, rotational and coupled diffusion

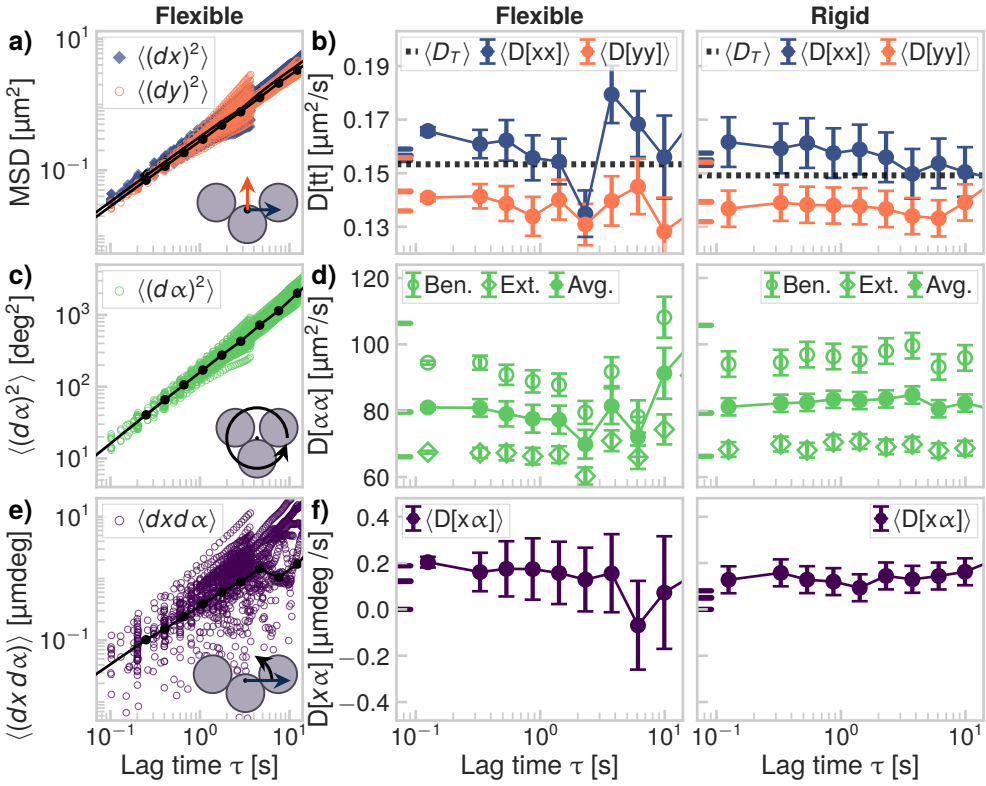

Figure 5.9: **Comparison between rigid and flexible trimers. a)** Mean squared displacements in x and y for all flexible trimers. **b)** Diffusivity in x and y as function of lag time for flexible (left) and rigid (right) trimers. The average translational diffusivity $\langle D_T(\tau_0 = 0.25\,\mathrm{s})\rangle$ (dotted lines) is $(2.7 \pm 0.3)\,\%$ higher for flexible clusters compared to rigid clusters. **c)** Mean squared angular displacements for all flexible trimers. **d)** Rotational diffusivity as function of lag time for flexible (left) and rigid (right) trimers. Bent configurations (Ben.) correspond to $\overline{\theta} < 120°$ and extended configurations (Ext.) to $\overline{\theta} \geq 120°$. **e)** Mean squared coupled displacements in x and α for all flexible trimers. **f)** Rotation-translation coupling in x and α as function of lag time for flexible (left) and rigid (right) trimers. In panels a, c and e, colored points are experimental data, black points and lines represent the fitted slopes. In panels b, d and f, numerical short-time diffusivities calculated based on Harvey et al.[107] are indicated by colored ticks on the y-axis, showing minimum, mean, and maximum shape-dependent values from bottom to top.

coefficients of flexible trimers to rigid trimers that are frozen in a particular shape and find that while they are qualitatively similar, there are experimentally measurable differences. Specifically, we measure that the average short time diffusion constant $\langle D_T(\tau_0 = 0.25\,\mathrm{s})\rangle$ of rigid trimers is $(2.7 \pm 0.3)\,\%$ lower ($(15 \pm 2)\,\%$ lower without friction scaling) than that of flexible trimers (Figure 5.9b, dotted lines), a small but measurable effect corroborated by the numerical models (see Section 5.2.3 and Figure 5.3). The rotational diffusion constants for flexible and rigid trimers are equal within the experimental uncertainty (Figure 5.9d), while the rotation-translation coupling mode between x and α is slightly higher for flexible trimers at the shortest lag time (Figure 5.9f). These findings agree qualitatively with numerical predictions[256–258] for hinged chains of spheres of higher aspect ratio (20:1 instead of 3:1 for the trimers). For these hinged rods, a 10 % increase in the translational diffusivity and a higher rotational diffusivity were found compared to rigid rods, which was attributed to hydrodynamic interactions between the subunits.[108,251]

The collective diffusion constant depends on size polydispersity

We have shown that freely-jointed trimers diffuse slightly faster than rigid trimers; their diffusion constant differs by approximately 3 %. When reporting such a small difference, it is important to exclude other effects that could lead to similar variations in the diffusion constant. Therefore, we here address the effect of size polydispersity on the average diffusion constant of a collection of particles. We consider an ensemble of particles, whose sizes are normally distributed around an average radius, $\bar{a}$, and with a standard deviation, σ. We assume that the particles exhibit Stokes diffusion so that each particle i has a size dependent diffusion constant

$$D_i = \frac{k_B T}{6\pi\eta a_i}.$$

Therefore, the smaller particles in the ensemble diffuse faster than the larger particles.

The experimental average diffusion constant of this ensemble of particles, $\bar{D}$, can be found by tracking the motion of many individual particles, calculating their individual diffusion constants and averaging those. One might assume that this average diffusion constant equals the diffusion constant of a monodisperse sample of particles with the same average size, but this turns out to be generally not true:

$$\bar{D} \neq \frac{k_B T}{6\pi\eta\bar{a}} \equiv D_{\bar{a}}.$$

The reason for this inequality is that the diffusion constant scales nonlinearly with size. Therefore, the diffusion constants of small particles are weighted more heavily than those of large particles, which skews the distribution of diffusion constant and shifts the average away from $D_{\bar{a}}$.

We asked how much the collective diffusion constant of a polydisperse sample would deviate from that of a monodisperse sample and how this deviation depends on size polydispersity. To this end, we first define the relative polydispersity as

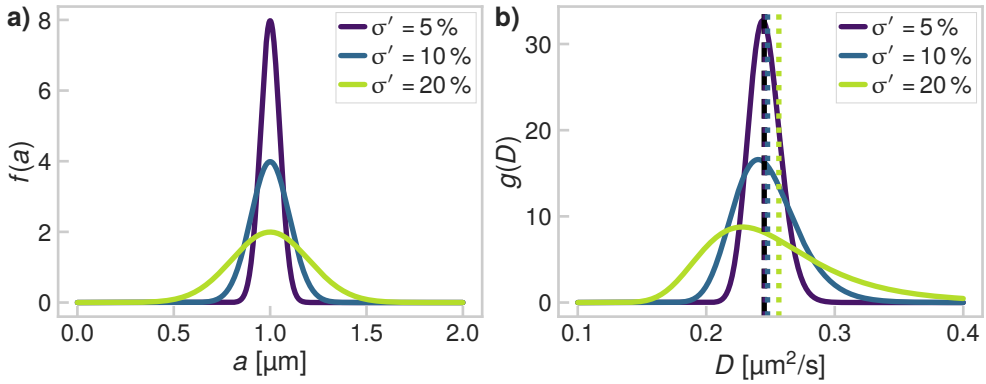

Figure 5.10: **The collective diffusion constant depends on size polydispersity. a)** Three hypothetical particle size distribution with an average particle radius of 1 µm and relative polydispersities of 5 %, 10 % and 20 %. **b)** The distributions in diffusion constant corresponding to the three particle size distribution in panel a. The average diffusion constants are indicated by dashed lines. The average diffusion constant of a monodisperse sample is indicated by a black dashed line.

$\sigma' = \sigma/\bar{a}$, which is a value between 0 and 1. The normalized distribution of particle sizes is then

$$f(a) = \frac{1}{\sigma'\bar{a}\sqrt{2\pi}} \exp\left[-\frac{1}{2}\left(\frac{a-\bar{a}}{\sigma'\bar{a}}\right)^2\right]. \tag{5.8}$$

Because the size is normally distributed and the diffusion constant scales with size as $1/a$, the diffusion constant exhibits a reciprocal normal distribution:

$$g(D) = \frac{D_{\bar{a}}}{D^2\sigma'\sqrt{2\pi}} \exp\left[-\frac{1}{2}\left(\frac{D_{\bar{a}}}{\sigma'}(1/D - 1/D_{\bar{a}})\right)^2\right]. \tag{5.9}$$

Figure 5.10a shows the hypothetical size distributions of three sets of particles with an average radius of 1 µm and relative polydispersities of 5 %, 10 % and 20 %. Figure 5.10b shows the diffusion constant distributions that correspond to these particle ensembles. Note that the diffusion constant is, unlike the size, not normally distributed. Instead, it has a tail of faster diffusion coefficients, corresponding to small particle sizes. Note also that the most probable diffusion constant shifts with polydispersity. This is also due to the $1/a$ scaling of the diffusion constant and can intuitively be explained by the fact that a range of large particles give a similarly small diffusion constant. This increases the probability of measuring this small diffusion constant and shifts the peak in the distribution. These properties of the distribution cause the average diffusion constant of a polydisperse sample (indicated by dashed lines in Figure 5.10b) to shift compared to the monodisperse case (indicated by a black dashed line). How much the diffusion constant is underestimated depends

on the size polydispersity. We intentionally chose large polydispersities to show the effect clearly. Note that at for a size polydispersity of 5 % the distribution of diffusion constants still looks rather symmetric.

The average diffusion constant of the particle ensemble is

$$\bar{D} = \int_{D=-\infty}^{D=\infty} D\, g(D)\, dD. \tag{5.10}$$

The integral in Equation 5.10 cannot be solved analytically, but we solved it numerically and compared it to the diffusion constant corresponding to particles with an average size $D_{\bar{a}}$. As integration limits we used 0 and $100 \times D_{\bar{a}}$ in order to probe all nonzero elements of the distribution function. We found that a 5 % polydispersity results in an underestimation of the diffusion constant by only 0.25 %. To underestimate the diffusion constant by 3 %, the relative polydispersity needs to be at least 17 %. We found that these results are independent of the particle size. This finding indicates that the measured 3 % increase of flexible trimers compared to rigid trimers cannot be due to size polydispersity alone, because the employed particles have a size polydispersity of only 2.6 %.

While polydispersity does not drastically alter the collective diffusion of microparticle suspensions, where σ' is typically around 5 %, it could play a large role in the diffusion of nanoparticles, where a σ' on the order of 100 % is not uncommon.[280] For example, gold nanoparticles with relative polydispersities on order of 10 % are considered very monodisperse and can only be made in a small parameter range.[281] Using Equation 5.10 we predict that the collective diffusion constant of a sample with 100 % polydispersity is 63 % larger than a monodisperse sample with the same average size, highlighting the importance of considering this effect in nanoparticle suspensions.

Flexibility-induced relaxation effects

The last way in which flexibility affects the diffusivity of a cluster is through the timescales on which effects of the initial cluster shape and orientation on the diffusive motions vanish. For rigid elongated particles it was shown that the timescale on which translational diffusivity in the x- and y-directions become equal with respect to the lab frame is set by the rotational diffusion time $\gamma_r = (D[\alpha\alpha])^{-1}$, with $D[\alpha\alpha]$ in rad^2/s.[91] To study this effect for our rigid and freely-jointed trimers, we analyze the motion of the clusters by defining the lab frame in such a way that the center of mass of the trimer at lag time $\tau = 0$ is at the origin and the body-centered x- and y-axes coincide with the original lab frame (see Figure 5.1c), an approach inspired by earlier works on rigid anisotropic particles.[97] Using the values for the short time rotational diffusion coefficients for compact and extended trimers, we find that for both rigid and flexible trimers $30\,\text{s} \leq \gamma_r \leq 60\,\text{s}$. Indeed, by looking at the translational (Figure 5.9b) diffusivity of rigid trimers, we see that the effect of shape on the diffusivity is preserved up to the maximum lag time we consider (10 s). The rotational

diffusivity (Figure 5.9d) of the rigid trimers stays constant within error (up to at least 10 s).

However, for flexible trimers, the story is different. There exists a second timescale that can average out orientation-dependent effects in diffusion: the timescale of shape changes, which we define as $\gamma_s = (D[\theta\theta])^{-1}$, analogous to the definition of the rotational diffusion time. Using the values for the short time flexibility coefficients for compact and extended trimers, we find that for our flexible trimers $8\,\mathrm{s} \leq \gamma_s \leq 35\,\mathrm{s}$. Therefore, we hypothesize that for flexible trimers, internal deformations lead to faster relaxation of the shape-dependency we observe at short lag times and therefore also the relaxation of differences between translational diffusion in the x- and y-directions.

Consistent with our hypothesis, the effect of the initial opening angle appears to be lost on a shorter timescale than what one would expect from the rotational diffusion time. In Figure 5.9d, the rotational diffusivity of flexible trimers is not constant in time, as is the case for rigid trimers, which shows that shape changes affect the diffusivity at longer lag times. The same effect can be seen in Figure 5.11b, where the cluster flexibility of compact and extended clusters become equal after about a second. Therefore, for lag times longer than 0.5 s, we only consider the shape-averaged diffusivities. As can be seen from the translational diffusivity (Figure 5.9b), the shape-averaged diffusivity in x and y become equal after 1 s to 3 s and this is also the timescale on which the rotational diffusivity is no longer constant (Figure 5.9d) and the translation-rotation coupling vanishes (Figure 5.9f). Moreover, we observe for both translational, rotational and translation-rotation coupled diffusion that after lag times larger than 2 s, larger fluctuations occur which we attribute to the effect of continuous shape changes (see Figure 5.9b, d and f).

Short timescale relaxation of differences between clusters in extended and compact conformations exist also for the conformational diffusion tensor elements. The flexibility (shown in Figure 5.11a, b) is smaller for trimers in bent conformations than in extended conformations and the difference vanishes after approximately 2 s due to shape changes. Figure 5.11b shows an overall decrease of flexibility with lag time, because the range wherein the joint angle can vary is bounded by the two outermost particles. Furthermore, the magnitude of $D[y\theta]$ (shown in Figure 5.11c, d), which represents the Brownian quasiscallop mode, vanishes on the same timescale of approximately 2 s, set by the conformational relaxation time $8\,\mathrm{s} \leq \gamma_s \leq 35\,\mathrm{s}$.

5.4 Conclusions

In conclusion, we studied the Brownian motion of flexible trimers and found features that are unique to flexible objects. We found a hydrodynamic coupling between conformational changes and translations perpendicular to the particle's long axis (y-direction), which we call the Brownian quasiscallop mode because of its resemblance to scallop propulsion at high Reynolds numbers. We found that this coupling persists over several seconds, a timescale relevant for biomolecular interactions, implying that it might affect the association of flexible proteins and other biomolecules. Secondly, we

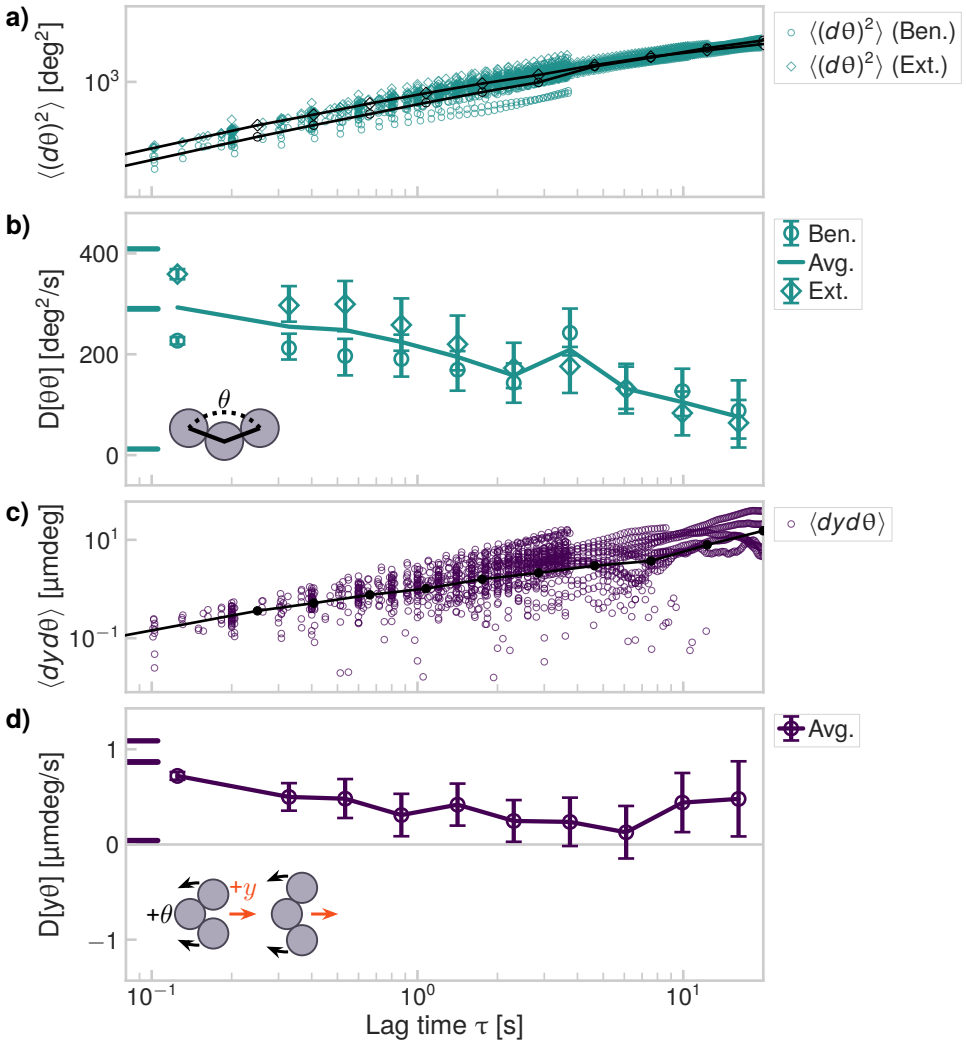

Figure 5.11: **Cluster flexibility and Brownian quasiscallop mode as function of time. a)** Mean squared angular displacements of θ for all flexible trimers. **b)** The flexibility decreases as function of lag time because of hard-sphere repulsion between the two outer particles. **c)** Mean squared coupled displacements of y and θ for all flexible trimers. **d)** The Brownian quasiscallop mode relaxes on a timescale of a few seconds because of conformational and rotational diffusion. In panels a and b, bent configurations (Ben.) correspond to $\overline{\theta} < 120°$ and extended configurations (Ext.) to $\overline{\theta} \geq 120°$. In panels a and c, colored points are experimental data, black points and lines represent the fitted slopes. In panels b and d, numerical short time diffusivities calculated based on Harvey et al.[107] are indicated by colored ticks on the y-axis, showing minimum, mean, and maximum shape-dependent values from bottom to top.

found that the long-time translational diffusion of the freely-jointed trimers was three to fifteen per cent higher than that of their rigid counterparts. This enhancement was predicted for hinged rods,[256–258] but contrasts with theoretical results on dumbbells of two hydrodynamically-coupled subunits, in which extensile shape fluctuations were shown to decrease the translational diffusion coefficient.[104,155] Further theoretical and experimental studies are needed to predict the effect of flexibility on diffusivity, since different internal degrees of freedom can have opposing effects. Finally, we showed that the transition from short- to long-time diffusion depends not (only) on the rotational diffusion time but mainly on a timescale related to conformational changes of the particle. We were able to describe our experimental findings using a hydrodynamic modeling procedure that combines bead-shell modeling with the approach of Harvey and coworkers.[107] We hope this work inspires other researchers to more confidently apply this method in the context of the diffusion of segmentally flexible systems such as biopolymers and proteins.

Acknowledgments

This chapter is based on the following publication:

Flexibility-induced effects in the Brownian motion of colloidal trimers.
R.W. Verweij*, P.G. Moerman*, N.E.G. Ligthart, L.P.P. Huijnen, J. Groenewold, W.K. Kegel, A. van Blaaderen and D.J. Kraft
Phys. Rev. Research, 2, 033136 (2020). doi:10.1103/PhysRevResearch.2.033136

This project has received funding from the European Research Council (ERC) under the European Union's Horizon 2020 research and innovation program (grant agreement no. 758383) and from the NWO graduate programme.

*These authors contributed equally.